Wear 308 (2013) 222–231

Contents lists available at ScienceDirect

Wear

journal homepage: www.elsevier.com/locate/wear

Multi-scale friction modelling for rough contacts under sliding conditions

D.K. Karupannasamy [a,b,*], M.B. de Rooij [b], D.J. Schipper [b]

[a] Materials innovation institute (M2i) - P.O. Box 5008, 2600 GA Delft, The Netherlands
[b] University of Twente, Faculty of Engineering Technology, Laboratory for Surface Technology and Tribology, P.O. Box 217, 7500 AE Enschede, The Netherlands

ARTICLE INFO

Article history:
Received 6 December 2012
Received in revised form
6 September 2013
Accepted 12 September 2013
Available online 14 October 2013

Keywords:
Deep drawing
Friction modeling
Asperity flattening
Ploughing
Multi-scale
Deterministic model

ABSTRACT

In Finite Element (FE) simulations of sheet metal forming (SMF), the coefficient of friction is generally expressed as a constant Coulomb friction. However in reality, the coefficient of friction at the local contact spot varies with the varying operational, deformation and contact conditions. Therefore, it is important to calculate the coefficient of friction under local contact conditions to better evaluate the formability of the sheet metal product. Friction at the local contact spot is largely influenced by the micro-mechanisms occurring at asperity level like shearing in the boundary layer, ploughing, surface deformation of the sheet metal surface and hydrodynamic lubrication. In this paper, a multi-scale contact model is developed for predicting the friction occurring in the SMF processes. The model describes the asperity flattening and ploughing phenomenon between the sheet metal and the tool which is predominant amongst the other friction mechanisms. The change occurring in the surface topography of the sheet metal during the deep drawing processes influences the ploughing process. An asperity flattening model for pure plastic conditions is used to describe this phenomenon. The developed model is analyzed with various sheet metal and tool surfaces. The result shows that the coefficient of friction is very much dependent on the surface topography of the interacting surfaces at low nominal contact pressures. At high nominal contact pressures, the surface topography influences less the friction. The coefficient of friction is also compared with tool surfaces of different roughness, bandwidth and surface lay. The coefficient of friction is found to be high for rough, low bandwidth and transversal anisotropic tool surfaces.

1. Introduction

In tribological problems, the traditional contact models of [1] and [2] are characterized by elastically and plastically deforming asperities for a fraction of the contact area at one roughness scale. However in SMF processes, the contact occurs between a smooth tool and a rough sheet metal surface. The surface roughness, S_q, of sheet metal is typically around 1–2 μm and the tool roughness is around 0.2–0.4 μm. The sheet metal surface deforms under normal loading and the fractional contact area increases. The tool indents into the deformed plateaus of the sheet metal surface. Due to the difference in the roughness scales, the contact occurring between the two surfaces can be assumed as follows (see Fig. 1 for a schematic representation of surfaces):

- At workpiece roughness level (sheet metal surface), the workpiece surface is soft and rough when compared to the tool surface.
- At tool roughness level, tool asperities indent and plough through workpiece due to sliding of sheet between the tools.

Ploughing occurs when there is a difference in the hardness of the material under contact. The harder material indents into the softer material and causes ploughing. Most of the metal forming process is often performed with the lubricant. The friction force is generated due to the energy losses by deforming the softer surface and shearing of the boundary layers formed due to lubrication.

Greenwood and Williamson [1] described an elastic contact model using statistical properties of the surface for the contact between nominally flat surfaces. The surface is assumed to have summits with a constant radius and a known summit density. The summit based contact models are suitable for a low fraction of area in contact. Pullen and Williamson [2] described a surface based plastic contact model assuming volume conservation. In the model [2], the asperity flattening process at high loads with the rise of asperities is modeled using statistical properties of the surface. Nayak [3] modeled plastic contact with the distribution of contact patches and holes (valleys) for the given separation using the statistical properties of the surface. He also found that the summit based models do not give the true contact area and the fractional contact area exceeds unity under conditions of

* Corresponding author at: Materials Innovation Institute (M2i), P.O. box 5008, 2600 GA Delft, The Netherlands. Tel.: +31534894325; fax: +31534894784.
E-mail addresses: d.karupannasamy@m2i.nl, k.dineshkumar@yahoo.co.in (D.K. Karupannasamy).

0043-1648/$ - see front matter © 2013 Elsevier B.V. All rights reserved.
http://dx.doi.org/10.1016/j.wear.2013.09.012

Nomenclature

Roman symbols

A	contact area of the asperity/surface [m^2]
B	parameter in Challen and Oxley's model [14] [dimensionless]
D_p	non-dimensional penetration depth of the asperity [dimensionless]
E	elastic modulus of the deforming surface [Pa]
F	frictional force [N]
H	hardness of the deforming material [Pa]
H_{ind}	indentation hardness of the deforming material [Pa]
K	kurtosis of the surface [dimensionless]
N	normal load [N]
P	contact pressure of the asperity/surface [Pa]
$R_{x,y}$	radius of the elliptical paraboloid in major and minor direction of the ellipse [m]
$S_{x,y}$	slope of the asperity in x and y directions [dimensionless]
S_q	RMS roughness value of the surface [m]
V	volume of the heights [m^3]
S_k	skewness of the surface [dimensionless]
a,b	major and minor radius of the elliptical paraboloid asperity [m]
a_{eff}	effective radius of the elliptical paraboloid asperity in sliding direction [m]
d	height of the asperity [m]
f_{hk}	interfacial friction factor, $f_{hk}=\tau_{\text{int}}/k$ [dimensionless]
h	separation distance of the surface from the mean plane [m]
k	shear strength of the deforming material [Pa]
$p_{x,y}$	pixel size of surface heights [m]
m	number of asperities/pixels/summits in contact [dimensionless]
$m_{0,2,4}$	moments of the surface [m^2],[dimensionless], [m^{-2}]
z	height of the pixel in the surface height data [m]

Greek symbols

α	fractional contact area [dimensionless]
β	attack angle of asperity with respect to sliding direction [rad]
γ	surface lay [dimensionless]
μ	coefficient of friction [dimensionless]
σ_κ	variance of curvature of the asperities in a surface [m^{-1}]
σ_s	variance of slope of the asperities in a surface [dimensionless]
σ_y	yield strength of the material [Pa]
σ_z	variance of heights in a surface [m]
τ	spatial separation [m]
τ_{int}	interfacial shear strength [Pa]
φ	orientation of the asperity w.r.t sliding direction [rad]
χ	shape factor for the asperity according to [13], ($\chi=0.8$) [dimensionless]
ψ	bandwidth parameter of the surface [dimensionless]

Subscripts and superscripts

avg	weighted average of the asperity parameter
cp	contact patch
nom	nominal
t	tool
wp	workpiece

Abbreviations

ACL	autocorrelation length
FE	finite element
FFT	fast Fourier transform
SMF	sheet metal forming

dominating plastic deformation. However, Nayak's analysis was focused on the development of contact patches. Following a statistical approach, he did not explain the detailed shape of the micro-contact patches which is critical for the friction prediction due to ploughing effects. Westeneng [4] developed a statistical contact model based on energy and volume conservation. He described the flattening and rising of asperities under plastic loading conditions. He also used the strain deformation models of Wilson and Sheu [5] and Sutcliffe [6] for contact area evolution due to bulk strain. Hol et al. [7] developed the numerical framework for the contact model of Westeneng [4] and applied it to large scale FE simulations. The important shortcoming of this contact model is the exclusion of hydrodynamic effects of the lubricant. Karupannasamy et al. [8] developed a mixed lubrication model to predict the lubrication effects during deep drawing processes. The model is based on [4] which use the statistical representation for the surfaces. One of the main disadvantages of the existing model is that the statistical representation of the surface which does not incorporate the direction dependency of the surface during sliding for the anisotropic surfaces and load independent characterization of the asperities. Ma et al. [9] developed a deterministic model by characterizing the micro-contact patches depending on the contact pressure to predict the coefficient of friction in an extrusion process due to ploughing of tool asperities through the extrudate. In their model, the contact between a flat soft surface and a rough hard surface was assumed. The characterization of micro-contact patches is adopted from the work of Masen et al. [10] for plastically deforming asperities in sliding contacts.

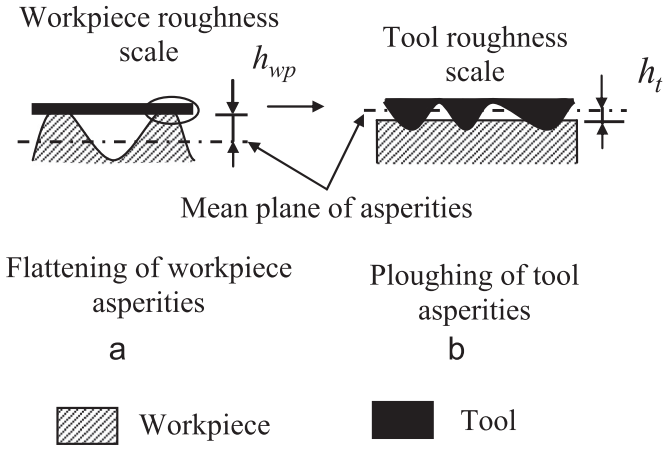

Fig. 1. Contact between workpiece and tool at (a) workpiece roughness scale and (b) tool roughness scale.

In this work, a multi-scale contact model is developed for rough contact situations between tool and workpiece in the metal forming processes. In contrast to existing models, the current model includes the roughnesses of both the sheet and the tool to explain the effects of surface properties like surface roughness,

surface lay and surface bandwidth parameter in the boundary lubrication regime. In order to simplify the analysis of the model, the surface deformation is considered only due to normal loading. The effects of bulk strain on asperity deformation as well as the hydrodynamic lubricant flow between the surfaces were already addressed in the earlier work [8]. The coefficient of friction could be influenced by the presence of oxide layers on the surface, repeated contact conditions, work hardening, etc. For simplicity, these influencing mechanisms are not considered. The main theme of this paper is limited to a friction model which explains the effect of surface geometry on the coefficient of friction. Results will be presented for several combinations of sheet metal and tool surfaces at different nominal contact pressures. It will be shown that the calculated coefficient of friction is very much dependent on the contact pressure and the detailed surface topography of the two contacting rough surfaces (sheet metal and tool surfaces).

2. Deterministic contact model

A deterministic contact model was developed by Ma et al. [9] for an aluminum extrusion process. The contact model includes only one roughness scale (tool roughness). In an aluminum extrusion process, the workpiece is soft and at high contact pressures it deforms onto the tool roughness resulting in a very high fractional contact area. However in SMF processes, the fractional contact area is typically lower and the roughness of the contacting surfaces is expected to be more important. Therefore, for deep drawing processes it is important to include both the roughness scales to predict the friction.

The multi-scale contact model is developed based on the work of Ma et al. [9] and Masen et al. [10] and applied to the SMF processes. The two scales are based on the roughness of the tool and workpiece surfaces. In the workpiece roughness scale, the workpiece is assumed to be rough and the tool to be flat. The smooth tool flattens the encountered workpiece asperities as shown in Fig. 1(a).

At the largest length scale (workpiece roughness scale), a deterministic contact model (see Section 3.1) is used to calculate the flattening of workpiece surface due to normal loading. At tool roughness scale, the tool is composed of micro-contacts ploughing through the flattened plateaus on the workpiece surface as shown in Fig. 1(b). The deterministic approach (see Section 3.2) is used to model the effect of size and shape of the ploughing tool asperities as described by Ma et al. [9]. The basic process in this model can be summarized as, (see Fig. 2 and Fig. A.1 in Appendix A)

1. Input of representative workpiece and tool surfaces.
2. Deformation of the workpiece surface.
3. Contact patch identification of the workpiece surface.
4. Mapping of tool asperities onto the identified workpiece contact patches.
5. Calculation of tool indentation by force equilibrium.
6. Characterization of tool asperity shape.
7. Calculation of the coefficient of friction.

2.1. Workpiece surface deformation model

The representative workpiece surface is taken from the DC06 steel sheet using a confocal microscope. The measured or numerically generated surface topography contains a matrix of heights/pixels of the surface. After the input of the surfaces as shown in Fig. 2(a), the contact patches are identified from the surface height data for a given surface separation, h_{wp}. The increase in contact pressure decreases the surface separation, h_{wp}. As a result, the size of the contact patches increases as shown in Fig. 2(b). In the asperity flattening model, the

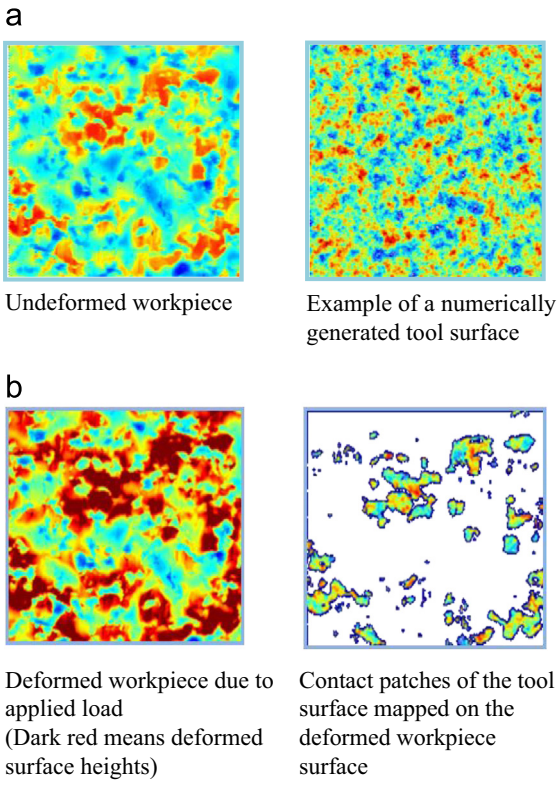

Fig. 2. (a) Representative workpiece and tool surfaces ($1 \times 1\ mm^2$) and (b) deformed workpiece surface and mapped tool surface.

identified contact patches are characterized to calculate the load carried for pure plastic conditions. During flattening, it is assumed that all the non-contacting asperities rise equally. The amount of rise of all non-contacting asperities is equal to the total flattening distance to maintain volume conservation. The contact patches are identified at a given separation distance using the binary image processing techniques. Each contact patch is identified by a cluster of pixels connected to its edge. Using the 4-connectivity criterion (at least 4 pixels connected together makes a contact patch) contact patches are identified. The pixels which do not form a contact patch are wiped out. The identified contact patches are characterized with elliptical paraboloids as described by Ma et al. [9] as shown in Fig. 3. The deterministic approach for the contact patches are described in a physically correct way than the statistical approach as shown in Fig. 3 (a). The connected pixels make an asperity which collectively deforms during the loading process as shown in Fig. 3(b). In the deterministic approach, the base of the asperity is defined by an ellipse with its major and minor axes length, ($2a$, $2b$) with an orientation angle, φ as shown in Fig. 3(b). Therefore, the entire surface is characterized into a number of elliptical paraboloids having specific shape properties. During asperity shape characterization, the volume and the area of the contact patch are preserved. The height of the asperity, d is obtained from the actual measured volume and area of the contact patch from the surface height data from the volume conservation.

$$d = \frac{2V_{cp}}{A_{cp}} \tag{1}$$

The volume and area of the contact patch calculated above the separation plane h is given as

$$V_{cp} = p_x p_y \sum_{i=1}^{m} (z_i - h) \quad A_{cp} = p_x p_y m \tag{2}$$

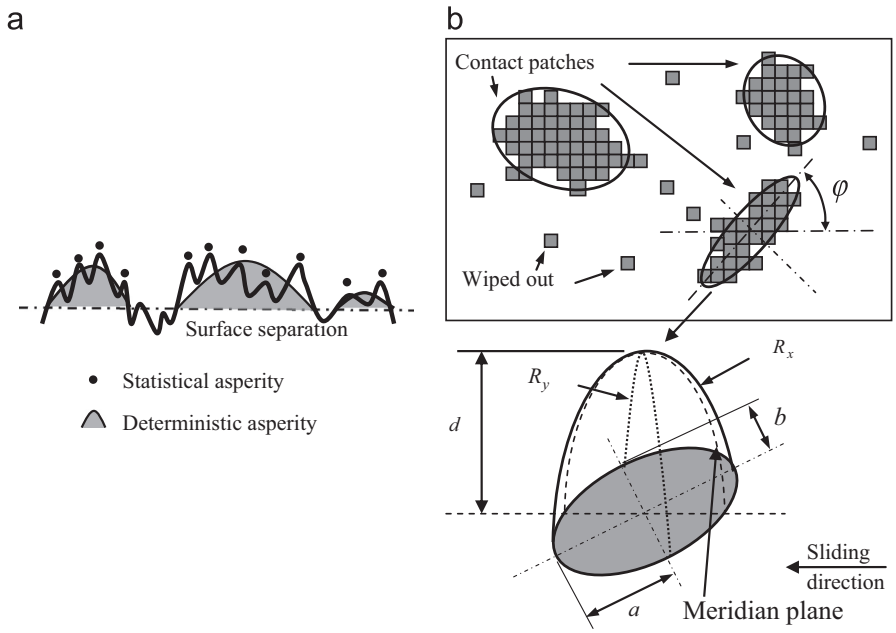

Fig. 3. (a) Comparison of statistical and deterministic surface characterization and (b) identification and characterization of asperities from Ma et al. [9].

where z is the height of a pixel in a contact patch, p_x and p_y are the pixel sizes in x and y direction and m is the number of pixels in contact.

During surface deformation under high contact loads, subsurface plasticity reaches the surface and full plastic deformation occurs. For pure plastic conditions, the pressure carried by an asperity is equal to the hardness, $P_{nom}=H$. For deep drawing materials, the workpiece is softer than the tool and it is assumed to deform in the full plastic mode. During the contact, it is fair to assume that the workpiece asperity will be in full contact with the tool during sliding. Abbott and Firestone [11] truncated the asperity at a given indentation depth to obtain the area of the plastic contact. In the similar way, the contact area,A_{wp}, and force,N_{wp}, for an elliptical paraboloid asperity under pure plastic conditions are given below according to [10]. From this method, the determined contact area is exactly equal to the area determined by Abbott and Firestone.

$$A_{wp} = 2\pi\sqrt{R_{x,wp}R_{y,wp}}d_{wp} \tag{3}$$

$$N_{wp} = HA_{wp} \tag{4}$$

with an iterative procedure, the separation plane, h_{wp} (as shown in Fig. 1(a)) is found. The nominal pressure, P_{nom} carried by the given surface is the sum of the contribution of the load carried by the individual asperities as follows:

$$P_{nom} = \frac{\sum_{i=1}^{m} N_{wp}^{i}}{A_{nom}} \tag{5}$$

2.2. Tool indentation model

The deformed workpiece contact patches are mapped on the tool surface as shown in Fig. 2(b). The surface heights of the contact patches are extracted from the given tool surface distribution. With the known tool surface height data of a contact patch, a paraboloid is constructed with an elliptical base of equal volume with the contact patches above the given tool indentation level, d_t (see Fig. 3). Thus each asperity of the tool coming into contact with the workpiece is uniquely characterized to calculate the friction forces. The tool separation plane, h_t (as shown in Fig. 1(b)) is found by means of an iterative procedure. The total applied load should be carried by all the tool asperities (m is the total number of contacting tool asperities) which are in contact with the workpiece. For sliding contact conditions, it is assumed that only front half of the tool asperity is in contact under pure plastic deformation. The contact area, A_t, and load, N_t, carried by an elliptical paraboloid asperity under fully plastic conditions according to [10] are given as

$$A_t = \pi\sqrt{R_{x,t}R_{y,t}}d_t \tag{6}$$

$$N_t = H_{ind}A_t \tag{7}$$

During indentation, hardness not only depends on the bulk material properties but also on the contact geometry. Indentation tests [15–18] show that the hardness increases with the decrease of the indentation size especially at the macro- and nano-indentations. Gao [17] derived an indentation model for spherical and conical shapes based on Johnson's expanding cavity model [18]. For pure plastic conditions with no strain gradient effects, the indentation hardness is given as

$$H_{ind} = \frac{2}{3}\sigma_y\left[\frac{7}{4} + \ln\left(\frac{1}{3}\frac{E}{\sigma_y}\cot\beta\right)\right] \tag{8}$$

2.3. Friction model

Once the contact patches of the tool surface are formulated, then the coefficient of friction, μ is calculated from the geometry of the asperity. The contribution of the plowing forces to the total friction force is dependent on the attack angle here represented by β. The attack angle of an asperity is separately calculated for each asperity depending on the orientation of the elliptical base shape, *scale120%φscale100%* with respect to the sliding direction as shown in Fig. 4. Hokkirigawa and Kato [13] extended the application of 2D slipline model of Challen and Oxley [14] to 3D scenario by introducing a shape factor *scale120%χscale100%* which was determined experimentally. The effective attack angle of an asperity, β prescribed by Ma et al. [9] depending on the orientation of the elliptical base with respect to sliding direction (i.e. along the meridian plane of the asperity as shown in Fig. 4) is given in the

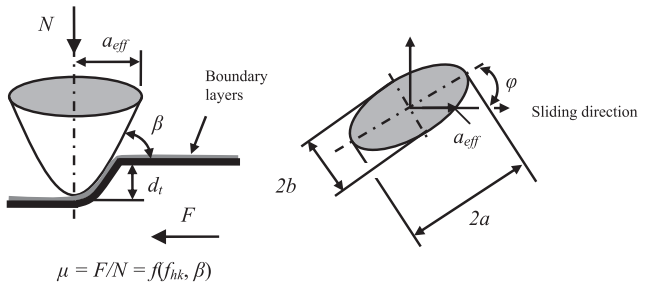

Fig. 4. Attack angle definition for the elliptical paraboloid asperity.

following equation:

$$\beta = 2\arctan\left(\frac{d_t}{\chi a_{eff}}\right) \tag{9}$$

The effective contact radius,a_{eff} of the elliptical paraboloid asperity is given as

$$a_{eff} = \left(\frac{ab}{\sqrt{a^2 \sin^2\varphi + b^2 \cos^2\varphi}}\right) \tag{10}$$

The coefficient of friction could be calculated from the arithmetic average attack angle of the asperities in contact with counter surface. In fact, taking the arithmetic average means that all the asperities are considered irrespective of its size. However, a bigger contact patch contributes more to the friction force than the smaller patch. Hence, an average effective attack angle, β_{avg} is calculated by means of weighting the effective attack angle of an individual asperity with the contact area of the micro-contacts as follows (according to [9]):

$$\beta_{avg} = \frac{\sum_{i=1}^{m} \beta^i A_t^i}{\alpha A_{nom}} \tag{11}$$

The coefficient of friction, μ is calculated from Challen and Oxley's model [14] with the input parameters from Table B.1 (see Appendix B). The coefficient of the friction is calculated with an interfacial friction factor, f_{hk} for boundary layers formed by the lubricant and average contact angle of the tool asperities, β_{avg}. The interfacial friction factor, $f_{hk}=\tau_{int}/k$ is dependent on the shear strength of boundary layers and deforming material. The friction factor is within range of $f_{hk}=0$–1. For well lubricated systems, the friction factor is low, $f_{hk}=0$–0.5. For boundary lubricated system or in case of lubricant failure, the friction is high $f_{hk} > 0.5$. In case of dry contact, the friction factor can reach values of 1 meaning that the shear strength of the interface is equal to the shear strength of the deforming material. The coefficient of friction is very much dependent on the attack angle of the asperity. Fig. C.1 in Appendix C shows the variation of friction with Challen and Oxley's model in different modes of deformation as a function of attack angle and interfacial friction factor. For small attack angle and lubricated systems ($f_{hk} < 0.5$), the coefficient of friction is low and the mode of deformation is plowing. In the plowing mode when there is no wear (for $\beta_{avg} < 45^\circ$), the coefficient of friction is given as

$$\mu = \frac{B \sin\beta_{avg} + \cos(\cos^{-1} f_{hk} - \beta_{avg})}{B \cos\beta_{avg} + \sin(\cos^{-1} f_{hk} - \beta_{avg})} \tag{12}$$

where

$$B = 1 + \frac{\pi}{2} + \cos^{-1} f_{hk} - 2\beta_{avg} - 2\sin^{-1}\frac{\sin\beta_{avg}}{(1-f_{hk})^{1/2}} \tag{13}$$

3. Results and discussion

For the calculations, workpiece surfaces are measured from six random spots of size 1 mm × 1 mm with a spatial resolution of 1 μm using a confocal microscope from the DC06 sheet metal at different spots. The properties of the measured workpiece surfaces (see Fig. D.1 of Appendix D) are listed in Table D.1 (see Appendix D). For this parametric study, various tool surfaces have been digitally generated by using the FFT techniques of Hu and Tonder [12] with different values for the roughness parameters as shown in Fig. D.2 (see Appendix D). The bandwidth parameter (see Eq. (15)) for the digitally generated tool surfaces is matched to the real tool surface. The surface properties are listed in Table D.2 (see Appendix D). The calculated coefficient of friction is shown in Figs. 5–8 for various applied nominal pressures. The results are shown for six different workpiece spots with the standard deviation. The friction values are shown for various tool roughness, S_q, surface lay, γ, and bandwidth parameter, ψ (see also Appendix B). The surface lay is defined by the ratio of autocorrelation length (ACL) of the surface in x and y directions.

$$\gamma = \frac{\mathrm{ACL}_x}{\mathrm{ACL}_y} \tag{14}$$

The bandwidth parameter is defined by the moments of power spectral density of the surface (m_0, m_2, m_4) as

$$\psi = \frac{m_0 m_4}{m_2^2} = \left(\frac{\sigma_z \sigma_\kappa}{\sigma_s^2}\right)^2 \tag{15}$$

The variation of the coefficient of friction is shown in Fig. 5 (a) for three different workpiece surfaces (1–3) with tool surface 1 which are found to be extremities in the friction values. The friction decreases with a higher nominal contact pressure for all three workpiece surfaces. As the contact pressure increases, the tool surface undergoes higher indentation. At high indentation levels, the tool asperities cluster together to form large and small number of blunt contact patches as shown in Fig. 5(b). This results in lower coefficient of friction. While at low pressures, the tool asperities form sharp contact patches resulting in high friction as seen in Fig. 5(b).

It can also be seen that if the same tool surface is in contact with different workpiece surfaces, the coefficient of friction shows different values. The difference can be explained with the formation of tool–workpiece contact patches and its contact geometry. At low contact pressures, the variation of the coefficient of friction is high as seen in Fig. 5(a). This variation in the friction decreases with the increase of the contact pressure. The degree of penetration, $D_P = d_t/a_{eff}$, of the tool varies more at lower contact pressures than at higher contact pressures as shown in Fig. 5(b). If the degree of penetration is high, then the sharp contact patches are formed. For workpiece surface 1 (symbol ○), the degree of penetration is the highest and it forms sharp contact patches resulting in higher friction. For workpiece surface 3 (symbol ◊), the degree of penetration is the least. Consequently, blunt contact patches are formed which results in lower friction.

The calculated coefficient of friction is compared for three different tool roughness as shown in Fig. 6. For rough tool surfaces, the asperities plough through the workpiece with a high attack angle. Hence, the coefficient of friction is high. However for smooth tool surfaces, the asperities are blunt which results in a low coefficient of friction.

In Fig. 7, the coefficient of friction is shown for transverse and longitudinal lay. A transverse lay results in sharper contacts with respect to the sliding direction and produces high friction. A longitudinal lay results in blunt contacts and produces a low

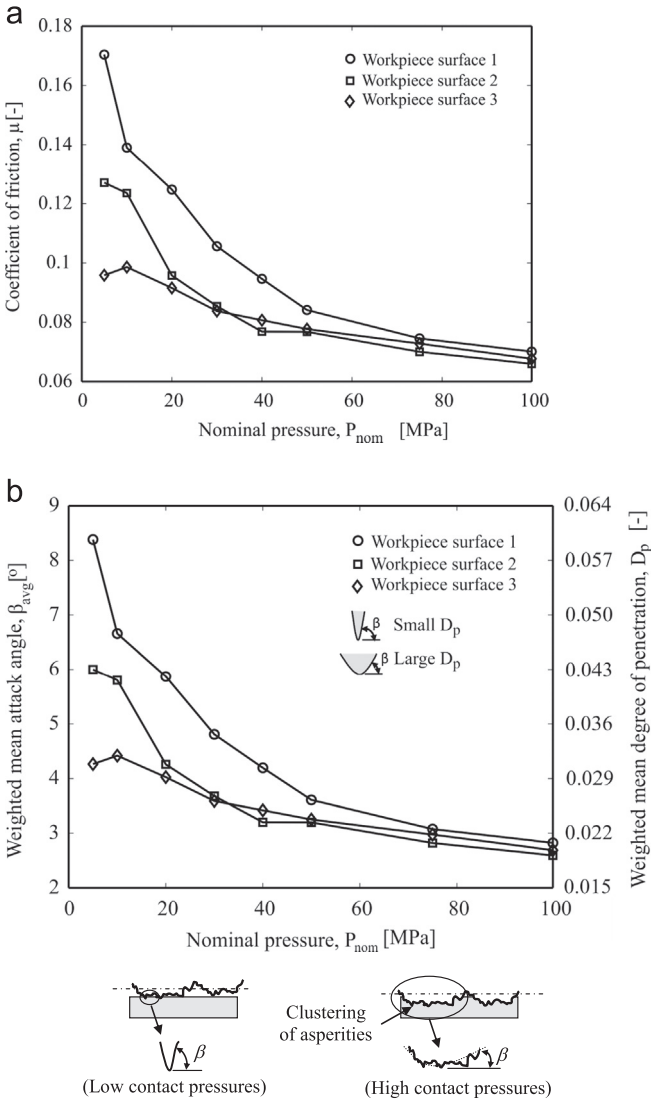

Fig. 5. (a) Calculated coefficient of friction for workpiece surfaces 1–3 with tool surface 1 and (b) degree of penetration of tool asperities and effective attack angle for various workpiece surfaces.

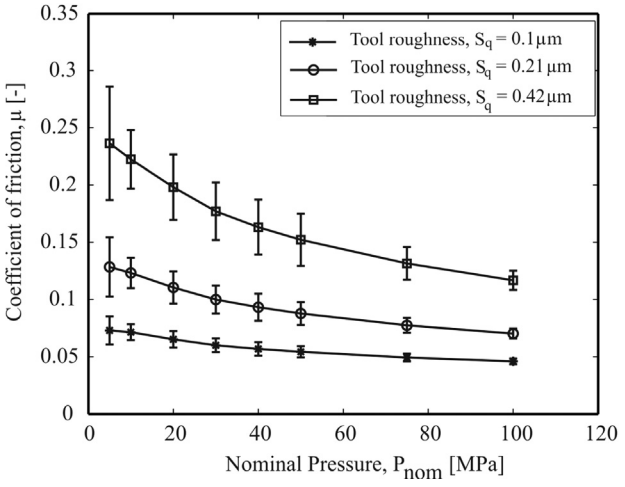

Fig. 6. Calculated coefficient of friction for various workpiece surfaces (see Table D.1) in contact with tool surfaces (see Table D.2) of different roughness.

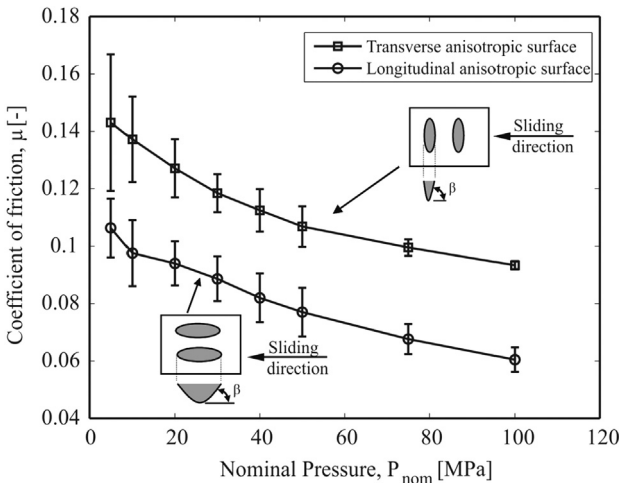

Fig. 7. Calculated coefficient of friction as a function of nominal contact pressures for tool surfaces of transversal and longitudinal surface lay.

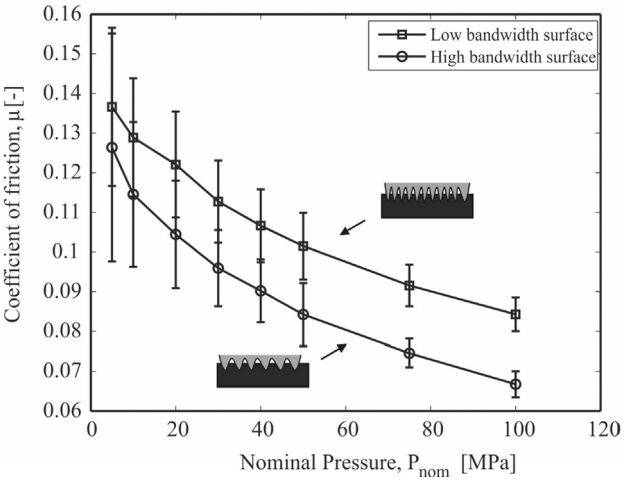

Fig. 8. Calculated coefficient of friction as a function of nominal contact pressures for tool surfaces of high and low bandwidth parameter.

friction. In Fig. 8, the results from the surfaces of low and high bandwidth parameters, ψ, are shown. Low bandwidth surfaces (spiky surfaces) results in a higher coefficient of friction than high bandwidth surfaces (smooth surfaces).

In Figs. 9–11, the comparison of the friction model with the experiments available in the literature is shown. Westeneng [4] studied the effect of tool roughness on the coefficient of friction using a linear friction tester developed by Ter Haar [19] for a constant nominal contact pressure as shown schematically in Fig. 9. The sheet material is held between a friction measuring device which consists of two hardened cylindrical rollers made of tool steel. In the experiments, a constant force is applied on the sheet material by rollers. The friction device can slide over the sheet material and it is driven by a servo motor. The typical sheet material EDT finished is with the material property shown in Table B.1 (see Appendix B) which is used for the experiments with pure oleic acid as lubricant. The experiment shows that the coefficient of friction is increased due to the increased plowing effects with the increase of the tool roughness. The friction model is used to calculate the coefficient of friction with the sheet material surface, numerically generated tool roughness of the same order of roughness. The interfacial friction factor is found to lie within a range of 0.5–0.9 for the boundary lubricated contacts with ploughing

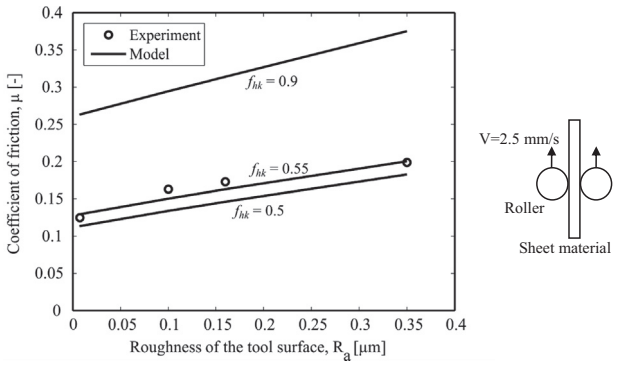

Fig. 9. Comparison of the friction model with experiments of Westeneng [4] for nominal contact pressure, P_{nom} = 156 MPa, as a function of tool surface roughness with steel sheet material.

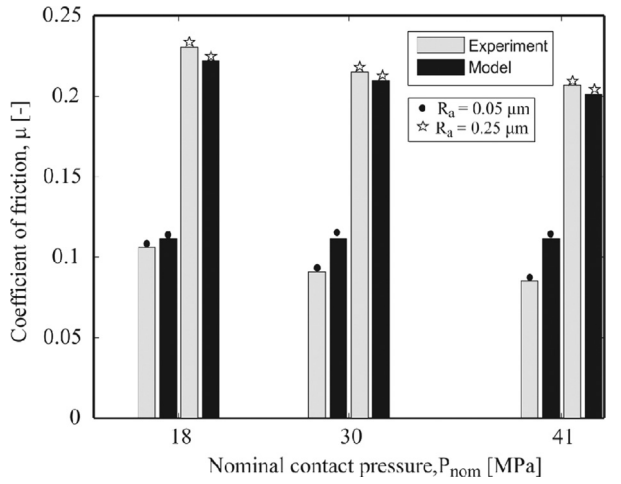

Fig. 10. Comparison of friction model with the experiments of Schedin [22].

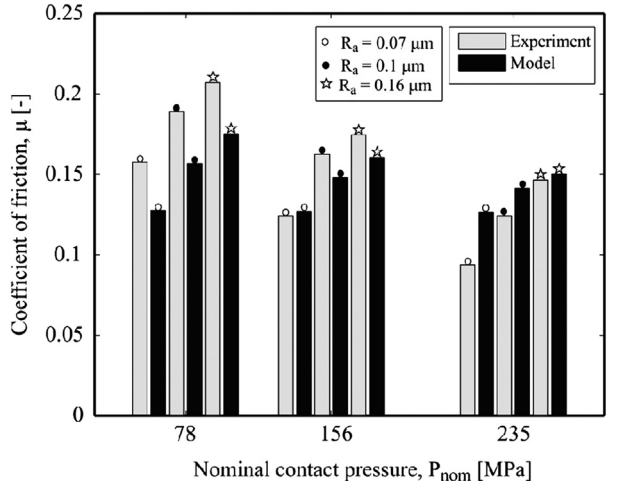

Fig. 11. Comparison of friction model with the experiments of Westeneng [4].

experiments using steel on single asperity scale according to [13,20] and [21]. The friction model predicts the trend of the coefficient of friction with the experiments quite well. In Fig. 9, the coefficient of friction is calculated as a function of tool surface roughness at a nominal contact pressure of P_{nom} = 156 MPa and compared with the experiments of Westeneng [4]. The interfacial friction factor, f_{hk} = 0.55, shows good agreement between the experiment and model. This interfacial friction factor is taken for further calculations.

Schedin [22] studied the effect of tool roughness with steel material low contact pressures with mineral oil as lubricant at a sliding velocity of 25 mm/s. The friction model is used with the surfaces of same order of roughness to compare with the experiments as shown in Fig. 10. The decreasing trend of the coefficient of friction with the increase in nominal pressure is observed in both the experiments as well as the model. The friction model predicts the coefficient of friction at high tool roughness well. When the surface roughness decreases, the trend of the coefficient of friction is still in agreement (see Fig. 6). However, the magnitude of decrease in friction is small with the contact pressure. The reason could be due to the fact that the asperity geometry characterization (using contact patches approach) which becomes less accurate for very low roughness conditions.

Westeneng [4] performed the experiments with tool roughness ranging from 7.6 nm to 0.16 μm with the strip tester at high nominal contact pressures. The friction model is tested with the surfaces of same order of roughness as shown in Fig. 11. The friction model predicts the trend of coefficient of friction as a function of contact pressure and tool roughness. The prediction capability again decreases at low roughness levels.

4. Conclusion

A multi-scale contact model is developed for the contact situations occurring in SMF processes for describing the friction at the local contact conditions under boundary lubrication regime. The model combines the surface deformation of the workpiece due to normal loading under pure plastic loading conditions with a detailed geometrical description of the tool asperities ploughing through the sheet surface. Results are shown for various combinations of tool and workpiece surfaces. It has been shown that the calculated coefficient of friction is strongly dependent on the micro-geometry of the tool and the workpiece, in particular at low values of the nominal contact pressure. At high nominal pressure, the coefficient of friction approaches to same value irrespective of the workpiece surface. Further it has been found that a rougher tool surface results in a higher coefficient of friction. A transverse surface lay produces higher coefficient of friction than longitudinal surface lay. Also a low bandwidth tool surface (spiky surface) results in a higher coefficient of friction as compared to high bandwidth surface. The friction model is compared with the experiments available in the literature and found to predict the trend of coefficient of friction with tool roughness and nominal contact pressure rather well. Although the model predicts the nature of surfaces, there are certain friction mechanisms necessary to improve the friction model. In ambient conditions, the surfaces are oxidized. The presence of oxide layers forms glaze during compaction and reduces the coefficient of friction. These oxide layers are removed during sliding and metal–metal contact occurs. During sliding, the surfaces are continuously changing with repeated contacts. In the repeated contacts, the asperity deformation and ploughing of the surfaces will be in the mixed mode of deformation (i.e. elastic–plastic). Hardening of the asperities during deformation is another important phenomenon which affects the contact area development at high contact pressure situations. The boundary layer friction factor chosen here is quite simple. The boundary layers are also continuously adsorbed and desorbed from the surface depending on the operational and environmental conditions. The friction factor

should depend on the probability of the contact between metal–metal combination, oxide layer and boundary layers due to lubrication. The contact model should incorporate these mechanisms to better the friction prediction.

Acknowledgments

This research was carried out under the project number MC1.07289 in the framework of the Research Program of the Materials innovation institute, The Netherlands (www.m2i.nl).

Appendix A

See Fig. A.1.

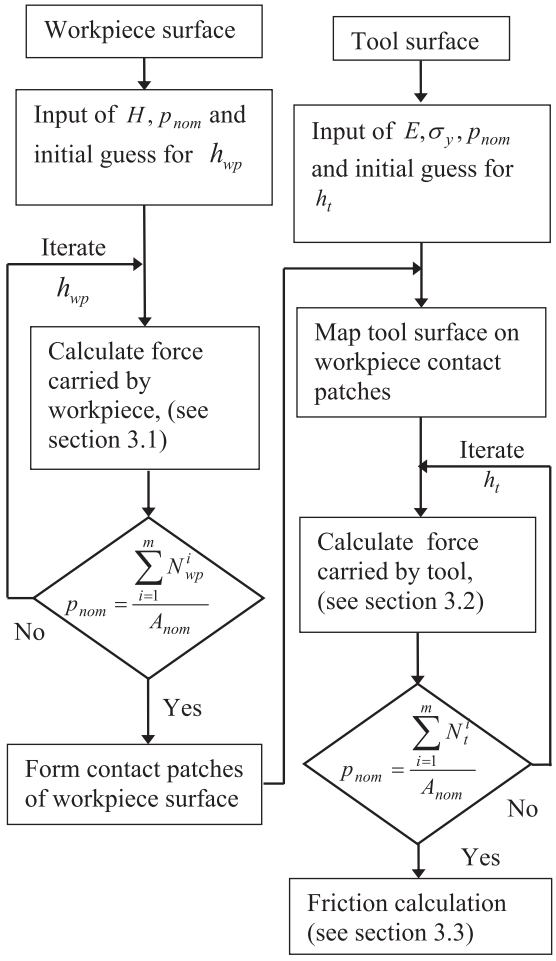

Fig. A.1. Flowchart for the friction model .

Table B.1
Input parameters for the calculations.

Parameters	Values
Workpiece hardness, H [MPa]	450
Elastic modulus, E [GPa]	210
Yield strength, σ_y [MPa]	180
Interfacial friction factor, f_{hk} [dimensionless]	0.1

Appendix B

See Table B.1.

The auto-correlation function for a surface profile with m summits is calculated as

$$\mathrm{ACF} = \frac{\sum_{i=1}^{m} z(x)z(x+\tau)}{m} \tag{B.1}$$

The slope of a summit is calculated from the surface height data in a discrete manner using finite difference method. The slope at a point in x and y direction of the surface is given as

$$S_x = \left|\frac{z(x,y)-z(x+\tau_x,y)}{\tau_x}\right|$$
$$S_x = \left|\frac{z(x,y)-z(x,y+\tau_y)}{\tau_y}\right| \tag{B.2}$$

The equivalent slope of the summit is the mean of the slope in x and y direction.

$$S = \frac{S_x+S_y}{2} \tag{B.3}$$

If the number of asperities are m, then the standard deviation of the surface slope is

$$\sigma_s = \sqrt{\frac{\sum_{i=1}^{m}(S_i-p)^2}{m}},\ \text{where } p = \frac{\sum_{i=1}^{m} S_i}{m} \tag{B.4}$$

The curvature of a summit obtained in discrete manner is given as

$$\kappa_x = \left|\frac{z(x-\tau_x,y)-2z(x,y)+z(x+\tau_x,y)}{\tau_x^2}\right|$$
$$\kappa_y = \left|\frac{z(x,y-\tau_y)-2z(x,y)+z(x,y+\tau_y)}{\tau_y^2}\right| \tag{B.5}$$

The equivalent curvature of the summit is the mean of the curvature in x and y direction

$$\kappa = \frac{\kappa_x+\kappa_y}{2} \tag{B.6}$$

The standard deviation of the surface curvature with m asperities is

$$\sigma_\kappa = \sqrt{\frac{\sum_{i=1}^{m}(\kappa_i-q)^2}{m}},\ \text{where } q = \frac{\sum_{i=1}^{m}\kappa_i}{m} \tag{B.7}$$

The input parameters for the friction model are shown in Table B.1.

Appendix C

Challen and Oxley's model uses the slipline analysis to describe the deformation of the surface due to the hard asperity in three different modes – ploughing, wear and cutting. For small attack angles and low friction factor, ploughing of soft surfaces occurs without any wear. For high attack angles and high friction factor, the wear mode occurs. For high friction factor with low attack angles, the cutting of softer surfaces occurs as in machining process. Fig. C.1 shows the coefficient of friction as a function of friction factor and attack angle.

The equations to calculate the coefficient of friction according to the mode of deformation is given below.

For ploughing mode

$$\mu = \frac{B \sin\beta + \cos(\cos^{-1} f_{hk} - \beta)}{B \cos\beta + \sin(\cos^{-1} f_{hk} - \beta)} \quad \text{(C.1)}$$

where

$$B = 1 + \frac{1}{2}\pi + \cos^{-1} f_{hk} - 2\beta - 2\sin^{-1}\left(\frac{\sin\beta}{(1-f)^{1/2}}\right) \quad \text{(C.2)}$$

For cutting mode

$$\mu = \tan\left(\beta - \frac{1}{4}\pi + \frac{1}{2}\cos^{-1} f_{hk}\right) \quad \text{(C.3)}$$

For wear mode

$$\mu = \frac{\{1 - 2\sin\beta^* + (1 - f_{hk}{}^2)^{1/2}\}\sin\beta + f_{hk}\cos\beta}{\{1 - 2\sin\beta^* + (1 - f_{hk}{}^2)^{1/2}\}\cos\beta + f_{hk}\sin\beta} \quad \text{(C.4)}$$

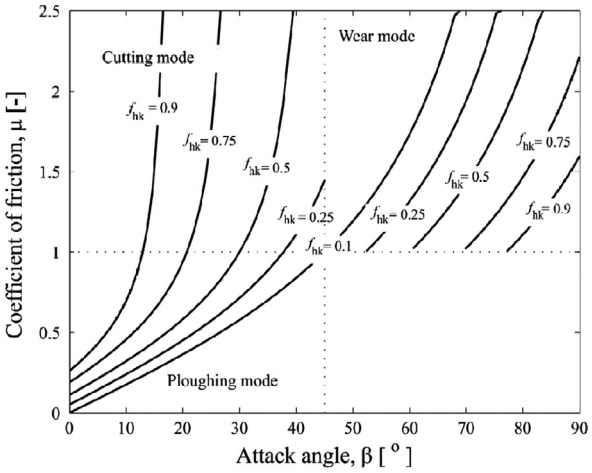

Fig. C.1. Influence of friction factor with the Challen and Oxley friction model .

where

$$\beta^* = \beta - \frac{1}{4}\pi - \frac{1}{2}\cos^{-1} f_{hk} + \sin^{-1}\frac{\sin\beta}{(1-f_{hk})^{1/2}} \quad \text{(C.5)}$$

Appendix D

See Figs. D.1 and D.2.

Surface topography of the DC06 sheet material (used in the calculations) is measured with a confocal microscope. The pixel size in both the directions is 1 μm.

Table D.1
Surface properties of the sheet material.

Workpiece surface	Surface roughness, S_q [μm]	Skewness, S_κ [dimensionless]	Kurtosis, K [dimensionless]	Surface lay, γ [dimensionless]
1	1.78	0.34	2.35	1.1
2	1.75	0.29	2.4	1.1
3	1.58	0.025	2.49	1.0
4	1.72	0.22	2.33	1.0
5	1.69	0.088	2.63	1.1
6	1.59	0.33	2.62	1.0

Table D.2
Properties of the generated tool surfaces.

Tool surface	Surface roughness, S_q[μm]	Surface lay, γ [dimensionless]	Bandwidth parameter, ψ [dimensionless]
1	0.21	1	34
2	0.42	1	34
3	0.1	1	34
4	0.21	0.3	34
5	0.21	3	34
6	0.21	1	16
7	0.21	1	44

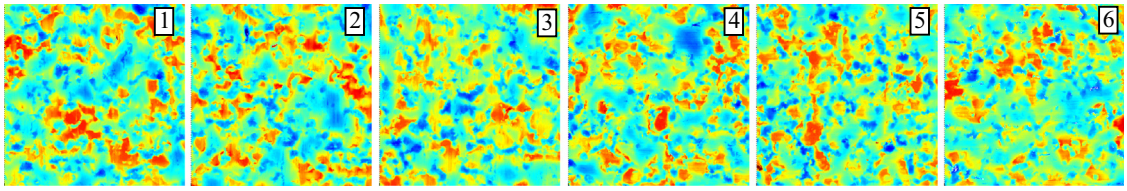

Fig. D.1. Measured surfaces of sheet material .

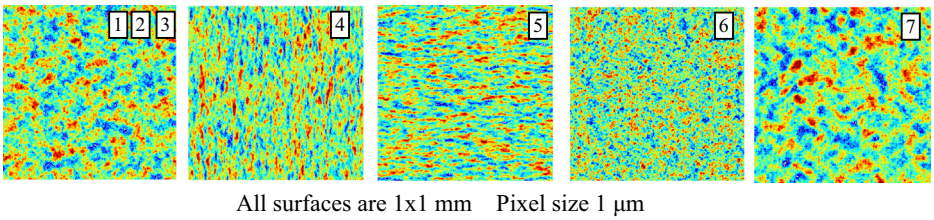

Fig. D.2. Topography of the numerically generated tool surfaces with different properties .

Surface topography of the numerically generated tool surfaces used in the calculation with different surface properties is mentioned in Tables D.1 and D.2.

References

[1] J.A. Greenwood, J.B.P. Williamson, Contact of nominally flat surfaces, Proc. R. Soc. London. Ser. A: Math. Phys. Sci. 295 (1966) 300–319.
[2] J. Pullen, J.B.P. Williamson, On the plastic contact of rough surfaces, Proc. R. Soc. London. Ser. A: Math. Phys. Sci. 327 (1972) 159–173.
[3] P. Nayak, Random process model of rough surfaces in plastic contact, Wear 26 (1973) 305–333.
[4] J. Westeneng, Modelling of contact and friction in deep drawing processes (Ph. D. thesis), University of Twente, The Netherlands, 2001.
[5] W.R.D. Wilson, S. Sheu, Real area of contact and boundary friction in metal forming, Int. J. Mech. Sci. 30 (1988) 475–489.
[6] M.P.F. Sutcliffe, Surface asperity deformation in metal forming processes, Int. J. Mech. Sci. 30 (1988) 848–867.
[7] J. Hol, M.V. Cid Alfaro, M.B. de Rooij, T. Meinders, Advanced friction modeling for sheet metal forming, Wear 286–287 (2012) 66–78.
[8] D.K. Karupannasamy, J. Hol, M.B. de Rooij, T. Meinders, D.J. Schipper, Modelling mixed lubrication for deep drawing processes, Wear 294–295 (2012) 296–304.
[9] X. Ma, M.B. de Rooij, D.J. Schipper, A load dependent friction model for fully plastic contact conditions, Wear 269 (2010) 790–796.
[10] M.A. Masen, M.B. de Rooij, D.J. Schipper, Micro-contact based modelling of abrasive wear, Wear 258 (2005) 339–348.
[11] E.J. Abbott, F.A. Firestone, Specifying surface quality – a method based on accurate measurement and comparison, Mech. Eng. 55 (1933) 569–572.
[12] Y.Z. Hu, K. Tonder, Simulation of 3-D random rough surface by 2-D digital filter and Fourier analysis, Int. J. Mach. Tools Manuf. 32 (1992) 83–90.
[13] K. Hokkirigawa, K. Kato, An experimental and theoretical investigation of ploughing, cutting and wedge formation during abrasive wear, Tribol. Int. 21 (1988) 51–57.
[14] J.M. Challen, P.L.B. Oxley, An explanation of the different regimes of friction and wear using asperity deformation models, Wear 53 (1979) 229–243.
[15] D. Tabor, Indentation hardness and its measurement: some cautionary comments, in: P.J. Blau, B.R. Lawn (Eds.), Microindentation Techniques in Materials Science and engineering, ASTM STP, 889, ASTM Press, Philadelphia, PA, 1986, pp. 129–159.
[16] J.G. Swadener, E.P. George, G.M. Pharr, The correlation of the indentation size effect measured with indenters of various shapes, J. Mech. Phys. Solids 50 (2002) 681–694.
[17] X.L. Gao, New expanding cavity model for indentation hardness including strain-hardening and indentation size effects, J. Mater. Res. 21 (2006) 1317–1326.
[18] K.L. Johnson, The correlation of indentation experiments, J. Mech. Phys. Solids 18 (1970) 115–125.
[19] R. Ter Haar, Friction in sheet metal forming – the influence of (local) contact conditions and deformation (Ph.D. thesis), University of Twente, The Netherlands, 1996.
[20] A.A. Torrance, J. Galligan, G. Liraut, A model of the friction of a smooth hard surface sliding over a softer one, Wear 212 (1997) 213–230.
[21] E.M. Kopalinsky, A.J. Black, Metallic sliding friction under boundary lubricated conditions: investigation of the influence of lubricant at the start of sliding, Wear 190 (1995) 197–203.
[22] E. Schedin, Micro-mechanisms of sheet-tool contact in sheet metal forming (Ph.D. thesis), Royal Institute of Technology, Sweden, 1991.